Energetics of neuronal signaling and fMRI activity

Natasja J. G. Maandag*[†‡], Daniel Coman*[†§], Basavaraju G. Sanganahalli*[†§], Peter Herman*[†§], Arien J. Smith*[†¶], Hal Blumenfeld[§‖]**, Robert G. Shulman*[†,††], and Fahmeed Hyder*[†§†††‡‡]

*Magnetic Resonance Research Center, [§]Quantitative Neuroscience with Magnetic Resonance, Departments of [†]Diagnostic Radiology, [‡‡]Biomedical Engineering, [‖]Neurology, and **Neurobiology, Yale University, New Haven, CT 06520

Contributed by Robert G. Shulman, October 11, 2007 (sent for review June 6, 2007)

Energetics of resting and evoked fMRI signals were related to localized ensemble firing rates (ν) measured by electrophysiology in rats. Two different unstimulated, or baseline, states were established by anesthesia. Halothane and α-chloralose established baseline states of high and low energy, respectively, in which forepaw stimulation excited the contralateral primary somatosensory cortex (S1). With α-chloralose, forepaw stimulation induced strong and reproducible fMRI activations in the contralateral S1, where the ensemble firing was dominated by slow signaling neurons (SSN; ν range of 1–13 Hz). Under halothane, weaker and less reproducible fMRI activations were observed in the contralateral S1 and elsewhere in the cortex, but ensemble activity in S1 was dominated by rapid signaling neurons (RSN; ν range of 13–40 Hz). For both baseline states, the RSN activity (i.e., higher frequencies, including the γ band) did not vary upon stimulation, whereas the SSN activity (i.e., α band and lower frequencies) did change. In the high energy baseline state, a large majority of total oxidative energy [cerebral metabolic rate of oxygen consumption (CMR_{O2})] was devoted to RSN activity, whereas in the low energy baseline state, it was roughly divided between SSN and RSN activities. We hypothesize that in the high energy baseline state, the evoked changes in fMRI activation in areas beyond S1 are supported by rich intracortical interactions represented by RSN. We discuss implications for interpreting fMRI data where stimulus-specific ΔCMR_{O2} is generally small compared with baseline CMR_{O2}.

awake | behavior | calibrated fMRI | glucose | glutamate

Noninvasive NMR and electrophysiological methods offer considerably different spatiotemporal results that presumably reflect the same cerebral activity. Localized energy consumption of neuronal and glial populations in MRI voxels has been evaluated (1), initially from ^{13}C MRS (2) and more recently from calibration of functional MRI (fMRI) (3). *In vivo* electrophysiological measurements of neuronal activity, from single neurons or large ensembles (4), are considered the gold standard of cerebral activity (5). Can measurements from these dissimilar techniques provide complementary insights into the working brain?

A promising convergence between these apparently different results relies on a universal thermodynamic principle, the fundamental relationship between the work done and the energy expended. Cerebral energy comes almost exclusively from glucose oxidation (6). Recent results have shown that the cerebral metabolic rate of oxygen consumption (CMR_{O2}) is almost completely dedicated to supporting work associated with synaptic activity (7, 8). Changes in CMR_{O2} from calibrated fMRI (9) are linear with changes in firing rates of a representative neuronal ensemble in the same voxel (10). This basic work/energy relationship has been extended by *in vivo* investigations (11, 12) that relate imaging energetics to the underlying neuronal activities.

Neuroimaging methods localize changes of task-induced activity by subtracting the prestimulus, or baseline, signal from the signal during the task period. The incremental signal (i.e., $\Delta S = S_{task} - S_{baseline}$) is generally a small fraction of the baseline signal. Because we now know that the blood oxygenation level-dependent (BOLD) signal reflects energy (13), and that the baseline energy supports neuronal activity (7), it is necessary to evaluate both incremental and baseline energies when comparing neuronal firing and CMR_{O2} (14). The total energy consumption of the stimulated state (i.e., sum of baseline plus increment), which supports neuronal activity of the entire ensemble, thereby designates a privileged role. The incremental energy cannot be used by itself to interpret neuronal functions, because it ignores the large spontaneous baseline energy that also serves undefined neuronal functions (15). Our approach has been to use noninvasive NMR methods to measure the energies of the baseline state and of its increments and then to relate the total energies of both the resting and stimulated states to the activities of a representative neuronal ensemble in the same volume element (16).

To explore neuronal foundations of baseline and incremental energetics, we conducted electrophysiological and fMRI studies in anesthetized rats at two very different anesthetized states, characterized by measurements of their baseline energies. The high energy baseline state, whose cerebral metabolic rate of glucose consumption (CMR_{glc}) is ≈10–20% lower than the awake state, was achieved by halothane (17). The low energy baseline state, where CMR_{glc} is reduced by ≈60% from the awake state, was accomplished by α-chloralose (18). The same forepaw stimulation was given in both states to excite the contralateral primary somatosensory cortex (S1). There were major differences between the two states in their fMRI activations and in the firing rates of a representative neuronal ensemble. Energetics of the ensemble at the different conditions were proportional to the measured energies of their volume elements. The work/energy relationship was expected from basic findings of neuroscience that oxidative energy supports neuronal activity (8) and from our previous experimental results in anesthetized rats (10). However, the findings of the current results is that the neuronal population could be divided into subgroups of slow and rapid signaling neurons [i.e., slow signaling neurons (SSN) and rapid signaling neurons (RSN), respectively] that correlated with the dissimilar fMRI activations observed between the two states.

Results

fMRI Activation Maps. Fig. 1 shows fMRI activation maps during forepaw stimulation. Although the majority of observed activations were cortical from either state, both the degree of localization in the contralateral S1 and the signal amplitudes [sup-

Author contributions: N.J.G.M., A.J.S., H.B., and F.H. designed research; N.J.G.M., D.C., B.G.S., P.H., and F.H. performed research; N.J.G.M., D.C., P.H., R.G.S., and F.H. analyzed data; and R.G.S. and F.H. wrote the paper.

The authors declare no conflict of interest.

[‡]Present address: Department of Anaesthesiology, University Medical Centre, 6500 HB, Nijmegen, The Netherlands.

[¶]Present address: Department of Neurosurgery, Mount Sinai Hospital, New York, NY 10021.

[††]To whom correspondence may be addressed. E-mail: fahmeed.hyder@yale.edu or robert.shulman@yale.edu.

This article contains supporting information online at www.pnas.org/cgi/content/full/0709515104/DC1.

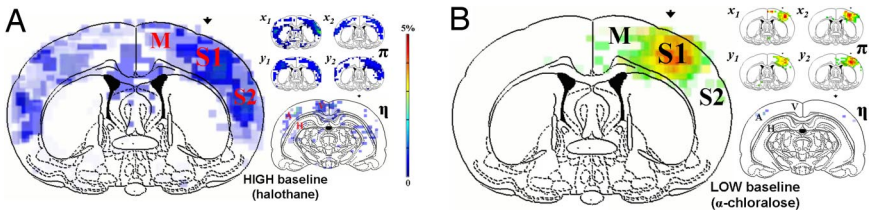

Fig. 1. fMRI activation maps during forepaw stimulation. The coronal maps are merged maps of single-run fMRI data from five rats to show overlap of averaged activities across subjects. All activation maps were thresholded at approximately the same value ($P < 0.02$) since the number of images varied slightly across studies. The contralateral side is shown by the arrow. (*A*) Sensory-induced activation maps with halothane showed activations in many regions, which included the primary (S1) and secondary (S2) somatosensory cortices and the primary and secondary motor (M) regions, as well as some lateral regions of the hippocampus (H) and some secondary area of the visual (V) and auditory (A) cortices (see η map, *Inset*). The contralateral S1 activity was stronger than in activations in other areas. (*B*) Sensory-induced activation maps with α-chloralose showed robust localized activations within the contralateral S1, with weaker activities within the contralateral S2 and M and no significant activations elsewhere (see η map in inset). (*Insets*) The π maps (anterior coronal slice) are single-run fMRI activation maps from two rats (i.e., subjects *x* and *y*) in two consecutive experiments to show reproducibility in S1, S2, and M areas. The x_1 and x_2 maps in *A* are from two runs from subject *x* under halothane, whereas the x_3 and x_4 maps in *B* are from two runs under α-chloralose from the same subject *x*. Similar data are shown for subject *y*. The η maps (posterior coronal slice) are merged maps of single-run fMRI activation maps from two rats (i.e., subjects *x* and *y*) to show overlap of averaged activities in V, A, and H across subjects. Other activated regions not shown are thalamus and perirhinal cortex (observed mainly under halothane). Refer to SI Table 2 for other details.

porting information (SI) Fig. 4] differed between the states. In the high energy baseline state (i.e., halothane), there were weak activations in the contralateral S1 as well as in other sensorimotor regions (Fig. 1*A*), which included the secondary somatosensory (S2) and primary/secondary motor (M) areas. In addition, there were activated posterior regions, which included lateral areas of the hippocampus (H) as well as some secondary areas of the visual (V) and auditory (A) cortices (see η map of Fig. 1*A*). Single-run fMRI activation maps showed variable patterns outside the contralateral S1, both across runs within the same subject and across different subjects (see π maps of Fig. 1*A*). Despite variability from scan to scan, the contralateral S1 activity was detected in a majority of the experiments (SI Table 2). A higher threshold (e.g., to exclude less activated voxels) only slightly reduced the size of some bilateral S1 clusters.

However, at low energy baseline state (i.e., α-chloralose), there was a robust localized fMRI activation within the contralateral S1, accompanied by much weaker activities within contralateral S2 and M (Fig. 1*B*). In posterior and/or ipsilateral regions of the brain, there were no significant activities (see η map of Fig. 1*B*). Single-run fMRI activation maps were quite reproducible, assessed both in terms of intra- and intersubject comparisons (see π maps of Fig. 1*B*). The strong contralateral S1 activity was detected in nearly all experiments (SI Table 2). Higher thresholding did not affect the S1 activation maps significantly, because the BOLD signal changes were quite large.

Behavior of the Neuronal Ensemble. Electrophysiological measurements provided neuronal firing rates (ν; 10-s bins) of 184 neurons in S1 (SI Fig. 5). Fig. 2 shows histograms of the ensemble firing rates in the different conditions (i.e., resting and stimulated conditions with both anesthetics shown in gray and black bars, respectively). We characterized two activity bands based on shapes of the different histograms. Activity of slow signaling neurons (SSN) was

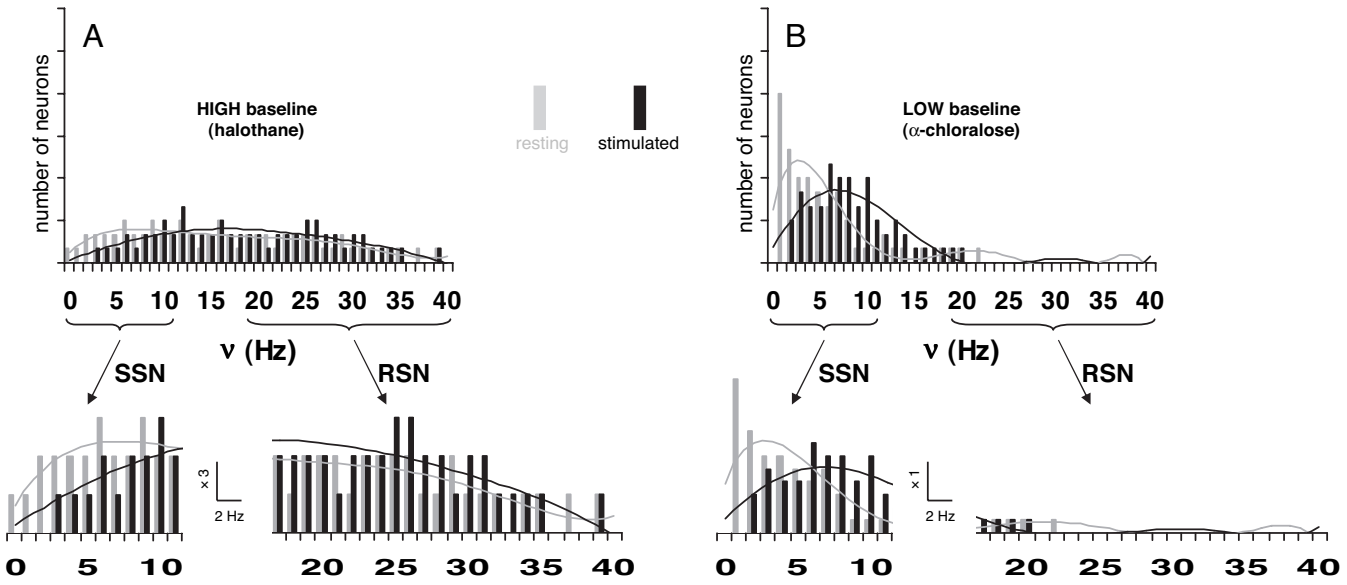

Fig. 2. Total activity represented by distribution of firing rate (ν; 10-s bins) in the S1 neuronal ensemble. By grouping the averaged firing rate for a given epoch (i.e., resting or stimulated period) from all recordings in the study, histograms were created to represent the behavior of the ensemble which comprised of 184 neurons. Activities of the same ensemble in the contralateral S1 are shown for resting (gray) and stimulated (black) conditions in the (*A*) high (halothane) and (*B*) low (α-chloralose) energy baseline states. Changes in the histograms are shown for the widespread firing rate distributions of the entire population (*Upper*; same vertical scales in *A* and *B*) and partitioned firing rate distributions (*Lower*; different vertical scales in *A* and *B*) revealing the slow and rapid signaling neurons, respectively (i.e., SSN and RSN). Refer to Table 1 and SI Fig. 5 for details.

Table 1. SSN and RSN activity of the neuronal ensemble

	High baseline (halothane)		Low baseline (α-chloralose)	
	Resting, %	Stimulated, %	Resting, %	Stimulated, %
SSN	34	35	84	87
RSN	66	65	16	13

Spike rate (ν; 10-s bins) grouped from all recordings in S1 for resting and stimulated epochs. SSN and RSN activities were defined as neurons with $\nu \lesssim 13$ Hz (i.e., α band and lower frequencies) and $\nu \gtrsim 13$ Hz (i.e., higher frequencies, including γ band), respectively. The partitioning frequency between the two bands was chosen to be 13 Hz, so that the sum of the SSN and RSN components added to the total population. Refer to Fig. 2 for details on RSN and SSN distributions and to SI Fig. 5 for details on induced responses of the ensemble. At high energy baseline state (i.e., halothane), ≈2/3 of the ensemble was involved with RSN activity, whereas the remaining fraction was dedicated to SSN activity. At low energy baseline state (i.e., α-chloralose), ≈1/8 of the population was occupied with RSN activity, whereas the remaining fraction of the ensemble was devoted to SSN activity.

defined by firing rates <13 Hz, whereas rapid signaling neurons (RSN) had firing rates in the range of 13–40 Hz.

Comparison of ensemble behavior between both unstimulated, or baseline, states shows that halothane (Fig. 2*A*) had slightly higher numbers in RSN than SSN (Table 1), whereas α-chloralose (Fig. 2*B*) was heavily weighted by SSN (Table 1). Stimulation produced only minor differences in the histograms for halothane (Fig. 2*A*), leaving the RSN activity nearly unchanged and only slightly shifting the SSN activity to higher frequencies. In contrast, there was a major difference between resting and stimulated histograms for α-chloralose (Fig. 2*B*). With α-chloralose, RSN activity was practically absent in both resting and stimulated states, whereas upon stimulation, there was a significant shift to higher frequencies of SSN activity. The percentage of SSN activity shift (upon stimulation) for α-chloralose (Fig. 2*B*) was similar to that observed with halothane (Fig. 2*A*); however, the significance of the change with α-chloralose was much higher, because a larger fraction of the population contributed to SSN activity (Table 1).

Energetic Demand of Neuronal Activity. Fig. 3 shows the energetic demand (CMR_{O2}) in the contralateral S1 neuronal ensemble. The "measured" columns were evaluated from 2-deoxyglucose autoradiography and/or NMR measurements (see *Materials and Methods*), whereas the other columns (i.e., "all," "SSN," and "RSN") were calculated from the histograms in Fig. 2 by weighting the number of neurons at any frequency with their firing rates on the assumption that energy expended by a neuron was linear with firing rate (Eq. **1**).

The measured CMR_{O2} for halothane (17, 19) and α-chloralose (18, 20) at rest were 3.86 ± 0.84 and 1.44 ± 0.30 μmol/g per min, respectively (see *Materials and Methods*). When normalized to the halothane resting state, the α-chloralose resting state was ≈63% lower (i.e., "measured" columns in Fig. 3*A*). The measured ΔCMR_{O2}% values for halothane and α-chloralose upon stimulation were 7 ± 18% and 62 ± 33% (see *Materials and Methods*) from each resting state, respectively (i.e., "measured" columns in Fig. 3 *B* and *C*).

Using Eq. **1**, the firing rates of the ensemble were related to their energy, and CMR_{O2} was calculated for all neurons in the histograms. The calculated CMR_{O2} using all neurons (i.e., "all" columns in Fig. 3*A*) for halothane at rest was normalized to 1.00 ± 0.08, so that the α-chloralose rest value was 0.34 ± 0.05. Upon stimulation, the calculated values of ΔCMR_{O2}% (using all neurons) for halothane and α-chloralose were 4 ± 10% and 67 ± 27%, respectively, from each resting state (i.e., "all" columns in Fig. 3 *B* and *C*). The calculated CMR_{O2} for all neurons were then partitioned into SSN and RSN activities (i.e., "SSN" and "RSN" columns in Fig. 3).

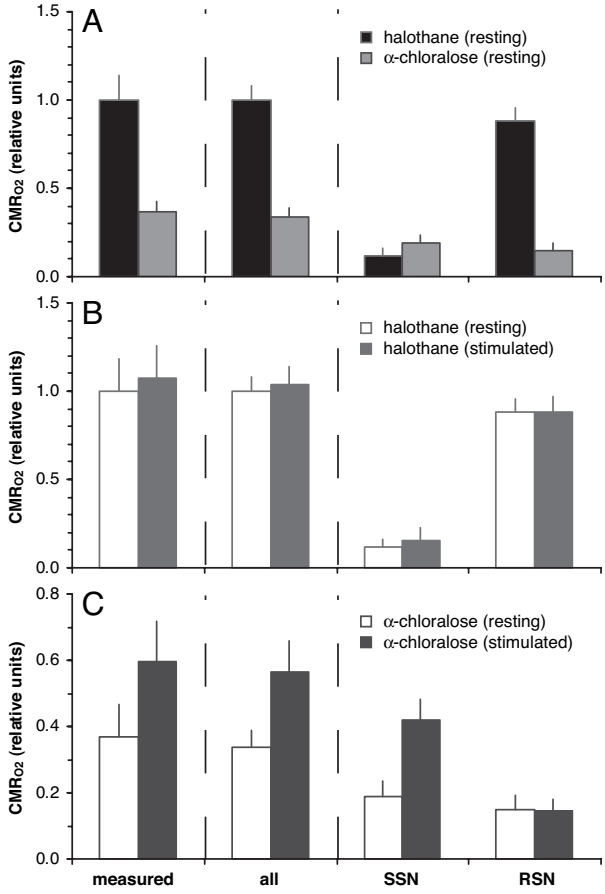

Fig. 3. Total energy demand (CMR_{O2}) in the S1 neuronal ensemble. Comparisons of energetic costs among (*A*) resting states under halothane and α-chloralose anesthesia, (*B*) halothane anesthesia at rest and during stimulation, and (*C*) α-chloralose anesthesia at rest and during stimulation. Data for the "measured" columns were estimated from 2-deoxyglucose autoradiography and/or NMR measurements (see *Materials and Methods*). Data for other columns were calculated from the histograms in Fig. 2 using Eq. **1**. The "all" columns were calculated by integrating the firing rate for each neuron for all neurons in the ensemble, whereas the "SSN" and "RSN" columns were calculated by integrating only the firing rate for the SSN and RSN portions of the ensemble, respectively. Refer to Table 1 for details. In all cases, good agreement was found between the "measured" and "all" columns. Partitioning of energetic cost between SSN and RSN portions of the ensemble suggests significantly different contributions under halothane and α-chloralose anesthesia. Energetic cost of RSN activity was almost unaffected by stimulation, whereas the SSN activity was more responsive to stimulation.

After normalizing all values to the calculated resting CMR_{O2} of halothane, excellent agreement was found between CMR_{O2} measured and calculated for all neurons (i.e., compare "measured" and "all" columns in Fig. 3). Comparison of CMR_{O2} between resting states for both anesthetics (Fig. 3*A*) shows that CMR_{O2} decreased by 63 ± 22% when measured and 66 ± 5% when calculated, switching from halothane to α-chloralose anesthesia. Under halothane (Fig. 3*B*), ΔCMR_{O2}% upon stimulation were 7 ± 18% when measured and 4 ± 10% when calculated. Similarly, under α-chloralose (Fig. 3*C*), ΔCMR_{O2}% upon stimulation were 62 ± 33% when measured and 67 ± 27% when calculated. Correspondence between CMR_{O2} measured and calculated (for all neurons) validated the relationship found between $\Delta\nu$ and ΔCMR_{O2} (10, 14) and established the validity of using the integration method of multiplying number of neurons with their firing rates (Eq. **1**).

Partitioning the total CMR_{O2} calculated into SSN and RSN activities (i.e., "SSN" and "RSN" columns in Fig. 3) provided insight into the relative energetic demands of these activities for the S1 ensemble. Under halothane, the SSN and RSN activities comprised 34% and 66%, respectively, of the population (Table 1), and the corresponding energy demands were 12% and 88% of the resting state total (i.e., "SSN" and "RSN" columns in Fig. 3*A*). Upon stimulation from halothane, the SSN and RSN activities comprised 35% and 65%, respectively, of the population (Table 1), and the energy demands were 15% and 85% of the stimulated state total (i.e., "SSN" and "RSN" columns in Fig. 3*B*). In contrast, under α-chloralose, the SSN and RSN activities comprised 84% and 16%, respectively, of the population (Table 1), and the corresponding energy demands were 56% and 44% of the resting state total (i.e., "SSN" and "RSN" columns in Fig. 3*A*). Upon stimulation from α-chloralose, the SSN and RSN activities comprised 87% and 13%, respectively, of the population (Table 1), and the energy demands were 74% and 26% of the stimulated state total (i.e., "SSN" and "RSN" columns in Fig. 3*C*). The SSN and RSN components roughly agree with α band and lower frequencies as well as higher frequencies including the γ band, respectively, and these types of low and high frequency signals have been measured by a variety of methods (5, 21–23).

Discussion

Measurable Properties of Baseline Activity. In functional imaging, the state of the system before stimulation is operationally defined as baseline. However, baseline is not the state of a system in a certain brain volume, which is comprised of synaptically connected neurons and astrocytes. Rather, baseline is the value of a measurable property of the unstimulated state. Depending upon the method, baseline could be evaluated by measuring CBF, or CBV, or CMR_{O2}, or the oxygen extraction fraction, or the BOLD signal acquired with a particular imaging sequence (e.g., gradient or spin echo). We have chosen the system's energy as the measurable property of baseline because our experiments can express energetics from measurements of both neuronal firing and calibrated fMRI (Fig. 3). With this designation, baseline CMR_{O2} is a property of the unstimulated (or resting) state of the neuronal system. Because the same S1 neuronal population is sampled by electrophysiological recordings, variation of baseline CMR_{O2} from halothane to α-chloralose anesthesia represents a shift in the properties of the neuronal system.

However, a measurable property defining a state of a thermodynamic system, which constitutes a large number of microscopic parts, does not specify the values of the subcomponents. For example, the temperature of a gas reflects the energy of the system, but the temperature value does not describe the individual particles which comprise the system. To quote Gibbs (24), energy defines "only a state which shall be indistinguishable from the previous one in its sensible properties." It should not come as a surprise, therefore, that a system of components within a certain brain volume is more heterogeneous than Gibbs's ideal gas. In fact, the present results allow us to decompose the measured energy into two components of the neuronal ensemble, i.e., the RSN and the SSN subgroups (Fig. 2). Furthermore correlations with the observed fMRI activations (Fig. 1) allow us to suggest how these neuronal components may have different roles in responding to stimuli and/or interacting with cortical regions.

fMRI Activations, Neuronal Signaling, and Energy Demand. We found major differences in the extent of dispersed fMRI activations between halothane and α-chloralose anesthesia. With halothane, there were activations in many cortical regions (Fig. 1*A*), which included homologous sensorimotor areas (i.e., S1, S2, M), as well as other distal areas (i.e., V, A, H) that are apparently beyond expectations from neuroanatomic hierarchy. Although repeated trials produced somewhat variable activations, the contralateral S1 activity was usually detected in most subjects (SI Table 2). With α-chloralose, the fMRI activations were reproducibly localized within the contralateral S1 with little spillover into other cortical regions (Fig. 1*B*). The most conspicuous difference between the unstimulated states of halothane and α-chloralose anesthesia (i.e., the high and low energy baseline states, respectively) was the dominant RSN activity/energy under halothane (Figs. 2*A* and 3*B*) compared with α-chloralose (Figs. 2*B* and 3*C*).

The SSN and RSN subgroups, defined by $\nu < 13$ Hz and in the range of 13–40 Hz, respectively, include frequencies of α and γ bands (4). γ band activity (i.e., high frequency) is observed under light anesthesia (25, 26) but rarely detected when animals are under deep anesthesia (27), whereas α band (and lower frequency) activity is dominant under deep anesthesia (28, 29). Detection of γ band activity under light anesthesia is not an anesthetic artifact, because awake animals show spontaneous activity in this range (27, 30). γ band activity tends to be correlated between homologous sensorimotor regions (e.g., S1, S2, and M) across hemispheres (26, 31) and can be modified by variations in global activity (32–34).

The somatosensory cortex is divided into primary (S1) and secondary (S2) areas that connect to primary and secondary motor (M) cortices (35). However, given the high degree of interconnectedness in the cerebral cortex (36), most cortical areas are believed to be reciprocally connected by intracortical innervations. Perception at the cortical level depends on mutual enforcement of exogenous (stimulus specific) inputs and endogenous (nonstimulus specific) inputs (37, 38). Under halothane, where RSN activity/energy (Figs. 2*A* and 3*B*) is the dominant fraction, fMRI activations were spread beyond the contralateral S1 (Fig. 1*A*), presumably because of the rich interconnected endogenous signaling within the cortex. This is quite similar to observations of sensory-induced activated homologous sensorimotor regions (e.g., S1, S2, M) only under lightly anesthetized conditions (39, 40). However, under α-chloralose, where there is less RSN activity/energy (Figs. 2*B* and 3*C*), fMRI activations were localized within the contralateral S1 and did not spread too much farther (Fig. 1*B*), presumably because of the reduced interconnecting activity. Robust localization of fMRI activation of the contralateral S1 during forepaw stimulation under α-chloralose has been successfully detected in many laboratories (41, 42). Our observation of less delocalized fMRI activity in the lower energy state is consistent with recent human experiments with and without sedation, corresponding to low and high energy baseline states, where loss of dispersed activations are detected in the low baseline (43–45).

There is a proposed correlation between the degree of RSN activity and the magnitude of CMR_{O2} in the baseline states, as seen in Fig. 3 and by Eq. **1**, where higher energy reflects higher firing rates. For the same population of neurons, as in our experiments, higher energies are necessarily expressed as higher firing frequencies. Hence our observation of higher RSN activities in a state of higher energy (i.e., halothane) reflects an obvious relation between total energy and SSN/RSN distribution in S1. Because other cortical regions show similar depression in CMR_{glc} from halothane to α-chloralose anesthesia (17–19), partition between RSN and SSN subpopulations in other cortical regions (e.g., S2, M, V) may have similar distributions. Although preliminary studies (data not shown) support this notion, further studies are needed to verify energy/activity correlations in different cortical regions.

Although energy is only one of the properties that can be used to characterize the state, the present results are consistent with high CMR_{02} being coupled to high RSN activity. Furthermore, we hypothesize that high RSN activity reflects high intracortical signaling and supports γ band activity observed under light anesthesia

(26, 31). On this hypothesis, in the low energy baseline state, RSN activity should be weaker throughout the cortex, which is consistent with γ band correlations not being detected under deep anesthesia (27). Studies are underway to assess the magnitude of RSN activity at other high energy baseline states.

Movement-free high resolution fMRI and electrophysiological data from rodents require, to some degree, restraint of the subject. In animal studies, this is usually achieved by anesthesia. The rats in our studies was also immobilized with paralyzing agents (*SI Text*) and the systemic physiology in the different anesthetized states was tightly controlled (SI Table 3). Anesthetics typically reduce brain energy consumption rather uniformly across regions (SI Fig. 6) and cortical energy decline is generally monotonic with anesthesia depth. It is generally accepted that most anesthetics, inhaled or injected, depress synaptic field oscillations as well as firing rates (46) and metabolism (47) of excitatory pyramidal cortical neurons possibly by enhancing $GABA_A$-mediated synaptic inhibition (48, 49). If halothane influences neurovascular and neurometabolic couplings differently than α-chloralose, fMRI activations could be different between the two states. Although exact molecular mechanism(s) of action for halothane and α-chloralose could vary (50), evidence from sensory stimulation studies suggests that neurovascular and neurometabolic couplings similar to the awake state are maintained by both of these anesthetics (SI Fig. 7). However, NMR studies of flow-metabolism coupling over a wide range of anesthetized states (51) and high resolution fMRI studies of the whole brain (52) are needed to avoid uncertainties.

In our limited data, acquired from only two anesthetized states, the relationship between RSN activity, γ band signaling, and the degree of fMRI activity localization is seen to vary with energy. We are hypothesizing that this energy/activity relationship will overwhelm any additional effects that might be introduced from other parameters (e.g., type of anesthetic used). Although further studies with different anesthetics are underway, our hypothesis is that the total energy is the dominant parameter that determines the RSN/SSN distribution of a finite neuronal population in a local region.

Energetic Basis of Baseline Activity. For a long time it was assumed, partly based on calculations from Creutzfeldt (53), that neuronal signaling requires only a negligible fraction of cerebral energy. This view of low energetic cost for neuronal signaling was further supported by early PET data suggesting that negligible CMR_{O2} increments (in the primary sensory region) were needed for function (54). Thus, the idea that brain spent little energy on function implicitly justifies using difference signals, representing small energy changes, to describe brain function allowing the large energies in the resting state to be ignored (55).

However, the "resting" brain is never at rest. Excitatory and inhibitory neurons in the cortex are never electrically silent, even in the absence of specific sensory (or cognitive) stimuli. High resting neuronal activity has been acknowledged since the earliest microscopic or macroscopic electrical recordings made from anesthetized or awake animals (56, 57). Nonetheless it took years of research, recently guided by ^{13}C MRS and calibrated fMRI, to establish the high energetic cost of activity at rest and then to show that differencing it away discards a large fraction of the total energy needed for function. Identification of the high energy consumption of neuronal activity for the unstimulated state (7, 8, 58) opened the door to hypotheses about the psychological processes supported by this activity.

We propose a model, based on our results, that relates energy in the SSN and RSN subpopulations to the localization of fMRI signals. At states of high energy baseline, a very large fraction of the energy supports the dominant RSN activity responsible for intracortical signaling across different regions. A sensory task stimulates a small SSN subpopulation which supports stimulus-specific inputs within the primary area. Ubiquitous intracortical interactions leads to widespread activations in other regions, and as much as possible, these regions have to be assessed without prejudice to preconceived neuroanatomical hierarchy. At states with low energy baseline, the RSN activity consumes a much smaller fraction of the energy reflecting reduced intracortical signaling. A task now stimulates the larger SSN subpopulation and requires much larger incremental energy to support stimulus-specific inputs within the primary area. However, the attenuated intracortical signaling does not spread activations into other regions and thus most of the activity remains within the primary area.

This model does not make *a priori* assumptions about the dedication of activities in the resting state to detailed psychological activities. Instead, it relates the observed SSN and RSN subpopulations to the observed BOLD signal localization (or lack thereof). In the present experiments, the distribution of energy between these two subpopulations, thought to be composed primarily of regular spiking pyramidal neurons (59), is presented as a function of the total energy of the resting state. The magnitude of this energy and its role in the breakdown into neuronal subpopulations are properties of the state and may depend on many factors, such as the anesthetic in use or other unmeasured physiological parameters that could alter the brain state, perhaps even while awake. The present breakdown of activity into two subpopulations of neuronal activity and energetics suggests their correlations with energetics and delocalization of functional activation patterns.

Materials and Methods

Animal Preparation for Multimodal MRI and Electrophysiology. All experiments were conducted on male Sprague–Dawley rats. A block design (off-on-off) electrical stimulation (2 mA, 0.3 ms, 3 Hz) was provided to each forepaw with a pair of copper electrodes. Each forepaw was stimulated separately. The stimulation period (0.5–5 min) was repeated between 2 and 5 times (in each anesthetized state) with at least 10-min resting periods. First functional studies under halothane ($\approx$1%) were conducted within $\approx$1.5 h. Anesthesia was then switched to α-chloralose with appropriate delay allowed for halothane clearance. Then functional studies under α-chloralose (45 $\pm$ 9 mg/kg per hour) began. For each rat, exactly the same stimulation protocol was applied, first under halothane and then under α-chloralose. Other details of experimental procedures are described in *SI Text*.

Energy Consumption of Neuronal Activity. We used literature values of CMR_{glc} (from 2-deoxyglucose autoradiography) and/or CMR_{O2} (from NMR) to estimate the energy demand in S1. It was necessary to convert the CMR_{glc} to CMR_{O2} by assuming (3) that glucose is fully oxidized. Resting state CMR_{glc} for halothane (17, 19) and α-chloralose (18, 20) in S1 were 0.64 $\pm$ 0.14 and 0.24 $\pm$ 0.05 μmol/g/min, respectively, and were converted to CMR_{O2} for each resting state value, which agree with ^{13}C MRS (SI Table 4). Previously measured CMR_{glc} changes in S1 upon stimulation (19, 20) with halothane (5 $\pm$ 21%) and α-chloralose (48 $\pm$ 26%) were converted to ΔCMR_{O2}%. With calibrated fMRI, we measured ΔCMR_{O2}% in S1 upon stimulation (SI Table 4) with halothane (13 $\pm$ 12%) and α-chloralose (90 $\pm$ 24%). Because of uncertainties associated with calibrated fMRI (*SI Text*) for the very different baseline states, as determined by their respective CBF/CMR_{O2} baseline value differences (SI Fig. 7), we averaged all measured ΔCMR_{O2}% values to minimize experimental bias.

Histograms of firing rate (ν; 10-s bins) from the electrophysiology data in S1 were converted to CMR_{O2} by assuming (8, 10, 14, 60) that oxidative energy is proportional to the number of cells firing at a given rate,

$$CMRO_2 = G \sum_i N_i \nu_i, \qquad [1]$$

where i spans the entire range of frequencies in the histogram, N_i is the number of cells at the ith frequency, ν_i is the ith frequency in the histogram, and G is a scaling factor that accounts for neuronal density and metabolic rate per neuron (8, 60). The SSN and RSN activity bands were defined as $\nu \lesssim 13$ Hz (i.e., α band and lower frequencies) and $\nu \gtrsim 13$ Hz (i.e., higher frequencies, including γ band), respectively, for the energetic calculations using Eq. **1**. The separating frequency between the two bands was chosen to be 13 Hz, so that the sum of the SSN and RSN components equaled the total histogram in every case.

ACKNOWLEDGMENTS. We thank Drs. Seiji Ogawa, Simon Laughlin, Afonso Silva, Bharat Biswal, and Joshua Brumberg for comments on earlier drafts of the manuscript and Drs. Douglas Rothman, Kevin Behar, Nikos Logothetis, and David Leopold for helpful discussions. This work was supported, in part, by the National Institutes of Health [National Institute of Mental Health (Grant R01 MH-067528, to F.H.), National Institute on Deafness and Other Communication Disorders (Grant R01 DC-003710, to F.H.), and National Institute of Neurological Disorders and Stroke (Grants P30 NS-52519, to F.H., and R01 NS049307, to H.B.)].

1. Hyder F, Patel AB, Gjedde A, Rothman DL, Behar KL, Shulman RG (2006) *J Cereb Blood Flow Metab* 26:865–877.
2. Shulman RG, Rothman DL, Behar KL, Hyder F (2004) *Trends Neurosci* 27:489–495.
3. Hyder F (2004) *Stroke* 35(Suppl I):33–39.
4. Buzsaki G, Draguhn A (2004) *Science* 304:1926–1929.
5. Buzsaki G (2006) *Rhythms of the Brain* (Oxford Univ Press, New York).
6. Siesjo BK (1978) *Brain Energy Metabolism* (Wiley, New York).
7. Sibson NR, Dhankhar A, Mason GF, Rothman DL, Behar KL, Shulman RG (1998) *Proc Natl Acad Sci USA* 95:316–321.
8. Attwell D, Laughlin SB (2001) *J Cereb Blood Flow Metab* 21:1133–1145.
9. Kida I, Kennan RP, Rothman DL, Behar KL, Hyder F (2000) *J. Cereb. Blood Flow Metab.* 20:47–860.
10. Smith AJ, Blumenfeld H, Behar KL, Rothman DL, Shulman RG, Hyder F (2002) *Proc. Natl. Acad Sci. USA* 99:10765–10770.
11. Uludag K, Dubowitz DJ, Yoder EJ, Restom K, Liu TT, Buxton RB (2004) *NeuroImage* 23:148–155.
12. Pasley BN, Inglis BA, Freeman RD (2007) *NeuroImage* 36:269–276.
13. Hyder F, Kida I, Behar KL, Kennan RP, Maciejewski PK, Rothman DL (2001) *NMR Biomed* 14:413–431.
14. Hyder F, Rothman DL, Shulman RG (2002) *Proc Natl Acad Sci USA* 99:10771–10776.
15. Shulman RG, Rothman DL, Hyder F (1999) *Proc Natl Acad Sci USA* 96:245–3250.
16. Shulman RG, Rothman DL, Hyder F (2007) *NeuroImage* 36:277–281.
17. Savaki HE, Desban M, Glowinski J, Besson MJ (1983) *J Comp Neurol* 213:36–45.
18. Dudley RE, Nelson SR, Samson F (1982) *Brain Res* 233:173–180.
19. Ueki M, Mies G, Hossmann KA (1992) *Acta Anaesthesiol Scand* 36:318–322.
20. Ueki M, Linn F, Hossman KA (1988) *J Cereb Blood Flow Metab* 8:486–494.
21. Gray CM, Singer W (1989) *Proc Natl Acad Sci USA* 86:1698–1702.
22. Destexhe A, Contreras D, Steriade M (1999) *J Neurosci* 19:4595–4608.
23. Volgushev M, Pernberg J, Eysel UT (2003) *Eur J Neurosci* 17:1768–1776.
24. Gibbs JW (1928) *Elementary Principles in Statistical Mechanics* (Yale Univ Press, London).
25. MacDonald KD, Barth DS (1995) *Brain Res* 694:1–12.
26. Jones MS, Barth DS (1997) *Brain Res* 768:167–176.
27. Franowicz MN, Barth DS (1995) *J Neurophysiol* 74:96–112.
28. Alkire MT (1998) *Anesthesiology* 89:323–333.
29. Jugovac I, Imas O, Hudetz AG (2006) *Anesthesiology* 105:764–778.
30. Gray CM, Viana Di Prisco G (1997) *J Neurosci* 17:3239–3253.
31. MacDonald KD, Brett B, Barth DS (1996) *J Neurophysiol* 76:423–437.
32. Engel AK, Konig P, Kreiter AK, Singer W (1991) *Science* 252:1177–1179.
33. Vaadia E, Haalman I, Abeles M, Bergman H, Prut Y, Slovin H, Aertsen A (1995) *Nature* 373:515–518.
34. Riehle A, Grun S, Diesmann M, Aertsen A (1997) *Science* 278:1950–1953.
35. Burton H (1986) in *Cerebral Cortex*, eds Jones EG, Peters A (Plenum, New York), Vol 5, pp 31–98.
36. Braitenberg V, Schuz A (1991) *Anatomy of the Cortex: Statistics and Geometry* (Springer, New York).
37. Ebner FF, Armstrong-James MA (1990) *Prog Brain Res* 86:129–141.
38. John ER, Prichep LS (2005) *Anesthesiology* 102:447–471.
39. Favorov OV, Whitsel BL, Chiu JS, Tommerdahl M (2006) *Brain Res* 1071:81–90.
40. Benison AM, Rector DM, Barth DS (2007) *J Neurophysiol* 97:200–207.
41. Xu S, Yang J, Li CQ, Zhu W, Shen J (2005) *NeuroImage* 28:401–409.
42. Gsell W, Burke M, Wiedermann D, Bonvento G, Silva AC, Dauphin F, Buhrle C, Hoehn M, Schwindt W (2006) *J Neurosci* 26:8409–8416.
43. Heinke W, Fiebach CJ, Schwarzbauer C, Meyer M, Olthoff D, Alter K (2004) *Br J Anaesth* 92:641–650.
44. Sperling R, Greve D, Dale A, Killiany R, Holmes J, Rosas HD, Cocchiarella A, Firth P, Rosen B, Lake S, *et al.* (2002) *Proc Natl Acad Sci USA* 99:455–460.
45. Dueck MH, Petzke F, Gerbershagen HJ, Paul M, Hesselmann V, Girnus R, Krug B, Sorger B, Goebel R, Lehrke R, *et al.* (2005) *Acta Anaesthesiol Scand* 49:784–791.
46. Antkowiak B (1999) *Anesthesiology* 91:500–511.
47. Gyulai FE (2004) *Curr Opin Anaesthesiol* 17:397–402.
48. Garrett KM, Gan J (1998) *J Pharmacol Exp Ther* 285:680–686.
49. Harris RA, Mihic SJ, Dildy-Mayfield JE, Machu TK (1995) *FASEB J* 9:1454–1462.
50. Lees G (1998) *Br J Anaesth* 81:491–493.
51. Hyder F, Kennan RP, Kida I, Mason GF, Behar KL, Rothman D (2000) *J Cereb Blood Flow Metab* 20:485–498.
52. Keilholz SD, Silva AC, Raman M, Merkle H, Koretsky AP (2004) *Magn Reson Med* 52:89–99.
53. Creutzfeldt OD (1975) in *Alfred Benzon Symposium,* Ingvar DH, Lassen NA, eds (Academic, New York), Vol VII, pp 21–46.
54. Fox PT, Raichle ME, Mintun MA, Dence C (1988) *Science* 241:462–464.
55. Posner MI, Raichle ME (1994) *Images of Mind* (Scientific American Library, New York).
56. Adrian ED (1941) *J Physiol* 100:159–191.
57. John ER (1961) *Annu Rev Physiol* 23:451–484.
58. Shulman RG, Rothman DL (1998) *Proc Natl Acad Sci USA* 95:11993–11998.
59. Connors BW, Gutnick MJ (1990) *Trends Neurosci* 13:99–104.
60. Lennie P (2003) *Curr Biol* 13:493–497.